Falx Cerebri Segmentation via Multi-atlas Boundary Fusion

Jeffrey Glaister[1(✉)], Aaron Carass[1,2], Dzung L. Pham[3], John A. Butman[4], and Jerry L. Prince[1,2]

[1] Department of Electrical and Computer Engineering,
Johns Hopkins University, Baltimore, MD 21218, USA
jglaist1@jhu.edu
[2] Department of Computer Science, Johns Hopkins University,
Baltimore, MD 21218, USA
[3] CNRM, Henry Jackson Foundation, Bethesda, MD 20817, USA
[4] Radiology and Imaging Sciences, NIH, Bethesda, MD 20892, USA

Abstract. The falx cerebri is a meningeal projection of dura in the brain, separating the cerebral hemispheres. It has stiffer mechanical properties than surrounding tissue and must be accurately segmented for building computational models of traumatic brain injury. In this work, we propose a method to segment the falx using T1-weighted magnetic resonance images (MRI) and susceptibility-weighted MRI (SWI). Multi-atlas whole brain segmentation is performed using the T1-weighted MRI and the gray matter cerebrum labels are extended into the longitudinal fissure using fast marching to find an initial estimate of the falx. To correct the falx boundaries, we register and then deform a set of SWI with manually delineated falx boundaries into the subject space. The continuous-STAPLE algorithm fuses sets of corresponding points to produce an estimate of the corrected falx boundary. Correspondence between points on the deformed falx boundaries is obtained using coherent point drift. We compare our method to manual ground truth, a multi-atlas approach without correction, and single-atlas approaches.

Keywords: Falx cerebri · Segmentation · MRI · Boundary fusion

1 Introduction

The falx cerebri is a sickle-shaped dura mater structure that extends into the longitudinal fissure and separates the left and right cerebral hemispheres [1]. Figure 1(a) shows a 3D rendering of a manually delineated falx (red) with the cerebrum overlaid as a gray transparency. Being a dural structure, the falx is stiffer than surrounding tissue and plays a vital role in supporting the brain by dampening brain motion inside the skull [6]. Early studies of the dynamic response of the human head showed the importance of including the falx in computational simulations by comparing models with and without the falx [12,13]. In particular, inclusion affected the frequency of the brain response and
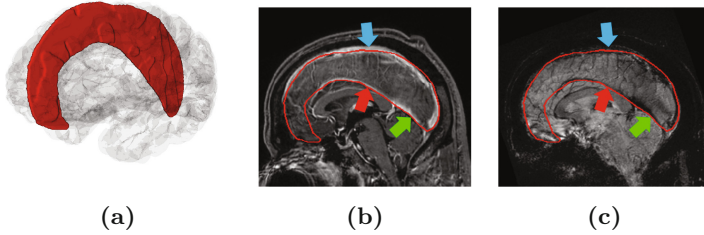
Fig. 1. Shown is a **(a)** 3D rendering of the falx (red) with the cerebrum overlaid as a gray transparency, the manual delineation of the falx (red contour) in **(b)** MPRAGE-PG, and **(c)** SWI. The inferior sagittal sinus (red arrow), straight sinus (green arrow) and superior sagittal sinus (blue arrow) are highlighted.

intracranial pressure during impact [12], and also altered the distribution of the intracranial pressure along the line of impact [13]. Inclusion of the falx is therefore necessary in the creation of accurate computational models of the brain for use in the study of traumatic brain injury.

To generate subject-specific models of the falx, it is common for the structure to be manually delineated from a sagittal slice in a T1-weighted (T1-w) magnetization prepared rapid gradient echo (MPRAGE) gadolinium-enhanced (MPRAGE-PG) magnetic resonance image (MRI) [3]. The sagittal slice can be either the midsagittal plane or central slice, whichever provides the best coverage of the longitudinal fissure. Delineating the falx in an MPRAGE-PG is feasible due to the presence of salient landmarks in the form of three sinuses that define the edges of the falx [1]. The inferior edge of the falx contains the inferior sagittal sinus and straight sinus and the superior edge contains the superior sagittal sinus. The anterior edge of the falx is attached to the crista galli and the posterior edge attaches to another dura mater structure, the tentorium cerebelli. Figure 1(b) shows an example of a sagittal slice with the falx delineated (red contour) on a MPRAGE-PG with the inferior sagittal sinus, straight sinus, and superior sagittal sinus highlighted with red, green, and blue arrows, respectively. However, an MPRAGE-PG is not always available since the contrast injection increases the risk of complications, and other modalities such as T1-w MRI or susceptibility-weighted MRI (SWI) do not provide much contrast between the falx and surrounding tissue, see Fig. 1(c) for an example.

Previous work on identifying the falx includes Chen et al. [5] which used computed tomography (CT) images to find the falx based on edge maps. Like MPRAGE-PG, the contrast between the falx and surrounding tissues is better in CT images, unlike in T1-w MRI and SWI. Chen et al. [4] proposed an atlas approach where a single atlas image is registered to the subject's T1-w and T2-w MRI, first by a rigid registration followed by a non-rigid registration. A falx model was transformed into subject space by applying the learned transforms. This method did not assume that the falx was contained within a single sagittal slice, thus it was able to find the falx in patients with large brain deformations. However, relying on a single atlas means that the subject falx is vulnerable

to registration errors, particularly when the atlas is highly dissimilar to the subject. Multi-atlas approaches overcome registration errors by applying a fusion algorithm to multiple atlases, with previous work by Glaister et al. [8] using the multi-atlas work of Huo et al. [9]. However, the thin nature of the falx makes directly applying multi-atlas approaches that rely on overlap-based label fusion methods difficult. Trained classifiers, such as deep neural networks, require a large set of manually delineated examples of the falx. Despite these methods, manual delineation of the falx on MPRAGE-PG is still accepted practice [3].

In this work, we propose a multi-atlas approach via boundary fusion to find the falx that uses T1-w MRI and SWI. An initial estimate of the falx is generated from the T1-w MRI using the gray matter labels that border the longitudinal fissure. We deformably register a set of atlases consisting of SWI and manual falx delineations, and then the coordinates of the boundary of the falx are transformed into the subject's space. We use coherent point drift [11] to find the sets of corresponding points between each of the atlases. These corresponding points are fused into a single boundary point using the continuous-STAPLE (Simultaneous Truth and Performance Level Estimation) algorithm [7]. The fused boundary is used to refine the initial falx by removing the mislabeled portions of the initial falx.

2   Method

2.1   Data and Preprocessing

Our data consists of 23 subjects with MPRAGE, MPRAGE-PG, and a SWI acquired using an EPI gradient echo T2*-weighted sequence; all data was acquired on a Siemens Biograph mMR 3T imaging platform. The images underwent standard pre-processing: inhomogeneity correction, skull stripping, and affine registration to an MNI atlas at 0.8 mm isotropic resolution. The SWI and MPRAGE-PG were affinely registered to the T1-w MRI in MNI space.

The MPRAGE-PG was used to create the manual delineations of the falx. The manual delineation protocol was a modification of the approach proposed in [3] to delineate the tentorium. Rather than assume that the falx lies in a single sagittal slice, a set of landmark points were manually selected on the falx throughout the brain. The landmarks were used to deform a plane using a thin-plate spline. The falx was manually delineated in this deformed plane using the intensities from the MPRAGE-PG.

To obtain an initial segmentation of the falx, a multi-atlas registration scheme is used to label the entire brain [14] with 30 Neuromorphometrics atlases (http://www.neuromorphometrics.com), which contain T1-w MRIs and label maps with 62 cortical labels per hemisphere [10]. The multi-atlas segmentation is refined to be consistent with the reconstructed cortical surface [9]. All gray matter (GM) labels are marched concurrently up to a distance of 5 mm and stop expanding when they reach another label or the edge of the skull mask. We consider the set of GM labels that occur adjacent to the longitudinal fissure and form two subsets of these GM labels consisting of those from the left hemisphere and those
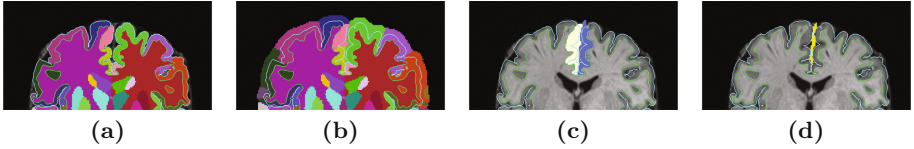
Fig. 2. Coronal view of the steps in the initial falx segmentation method: **(a)** the multi-atlas segmentation; **(b)** the fast march extended segmentation labels; **(c)** the label map showing voxels belonging to left hemisphere GM labels (pale yellow) and right hemisphere GM labels (blue); and **(d)** the initial falx segmentation (yellow). The inner and outer cortical surfaces are overlaid as green and cyan contours respectively.

from the right hemisphere. Then, for each voxel in the left hemisphere subset, any voxel with a neighbor that belongs to the right hemisphere subset is labeled as an initial falx voxel. This is repeated for voxels in the right hemisphere and the union of the results from both hemispheres is taken to be the initial falx. Figures 2(a)–(d) illustrate the steps to produce the initial falx.

2.2   Point-Set Correspondence

We refine our initial falx estimate with a multi-atlas registration scheme. Due to the small size of our data pool, we use one data set as the subject and the other four data sets with manual falx delineations as atlases. The atlases used to label cortical and subcortical structures in Sect. 2.1 are not used here because they do not have the falx labeled, nor do they have imaging modalities suitable to generate delineations of the falx. The atlas SWI are deformably registered to the subject SWI using the ANTS registration package [2]. The SWI are used because the sinuses are visible, which improves the registration in the longitudinal fissure. The falx boundary voxels from the atlas are transformed into the subject space using the learned deformation. To simplify the remaining steps, we also project these points onto a sagittal plane (encompassing the longitudinal fissure), turning the fusion problem into a 2D problem. The output of this step is transformed boundary coordinates $\mathcal{B}_i = \{\boldsymbol{b}_{i,j}\}$, where $\boldsymbol{b}_{i,j} \in \mathbb{R}^2$ is the jth boundary coordinate for the ith atlas. An example of the boundary coordinates from the four atlases after deformation is shown in Fig. 3(a) as differently colored dots.

To apply a fusion method to the boundary coordinates, it is necessary to determine the set of boundary coordinates that correspond with each other across the atlases. To achieve this, we use coherent point drift (CPD) [11], a point-set registration algorithm. First, we choose one atlas as the target atlas T for all the CPD registrations and the other atlases are moving atlases. For the ith moving atlas, the points in that atlas are considered as Gaussian mixture model (GMM) centroids while the points in the target atlas are considered as being generated from the GMM. CPD uses an Expectation-Maximization algorithm to find the optimal locations of the GMM centroids that maximize the likelihood. The non-rigid transformation in CPD uses a displacement function
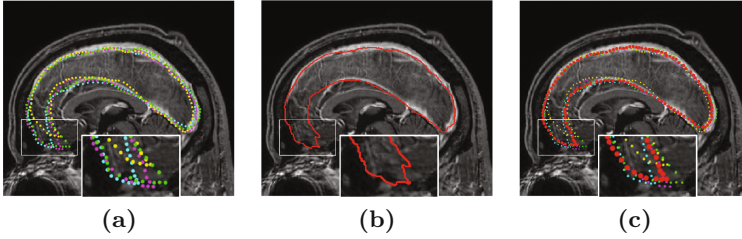
Fig. 3. (a) Yellow, green, magenta, and cyan points show the boundary coordinates after deformable registration from the four atlases, overlaid on the MPRAGE-PG. **(b)** Fused boundary (red contour) using traditional STAPLE. **(c)** Fused boundary coordinates (red dots) using continuous-STAPLE. The white rectangle shows an area of interest.

which is constrained with a motion coherence. In the Expectation step, the correspondence probability $p_{k,j}^i$ between points $\boldsymbol{b}_{T,k}$ and $\boldsymbol{b}_{i,j}$ is computed. After convergence, the probabilities are used to find $c_{i,k}$, the index of boundary coordinate in the ith atlas that corresponds to the kth boundary coordinate in the target atlas. CPD is repeated for all remaining atlases to compute the correspondence. Given these correspondences, we can establish a point-set correspondence among all the atlases to the chosen target atlas. That is, the set of points that correspond with $\boldsymbol{b}_{T,k}$ from the target atlas are $\{\boldsymbol{b}_{i,c_{i,k}}\}$, with i indexing over the moving atlases. It is important to note that only the coordinate correspondences are used and not the deformed CPD coordinates. In this work, we choose the first atlas as the target atlas.

2.3   Boundary Fusion and Final Falx

Once correspondence between sets of boundary coordinates is established, the boundaries are fused by applying the continuous-STAPLE algorithm. Continuous-STAPLE is an algorithm to probabilistically estimate the truth values from a set of atlases based on their estimated performance level. Traditional STAPLE methods rely on overlap between the structures, which is scarce in 3D due to the thin nature of the falx. Applying the traditional STAPLE algorithm to the falx contours projected on the sagittal plane produces a shape inconsistent with that of a real falx (see Fig. 3(b)). Continuous-STAPLE models the input vectors as observations of the hidden true vectors and employs an Expectation-Maximization algorithm to estimate the true vectors and performance parameters for each atlas. The output of continuous-STAPLE is a list of fused boundary coordinates, $\mathcal{B}_f = \{\boldsymbol{b}_j\}$, where the jth boundary coordinate $\boldsymbol{b}_j$ is the estimated fusion of $\{\boldsymbol{b}_{i,c_{j,l}}\}$. An example of the final boundary coordinates is shown in Fig. 3(c) as a set of red dots.

Finally, we incorporate our refined falx boundary into our initial falx estimate. As the refined boundary has been projected on the sagittal plane, we modify the initial falx in a similar manner. The initial falx is projected onto the
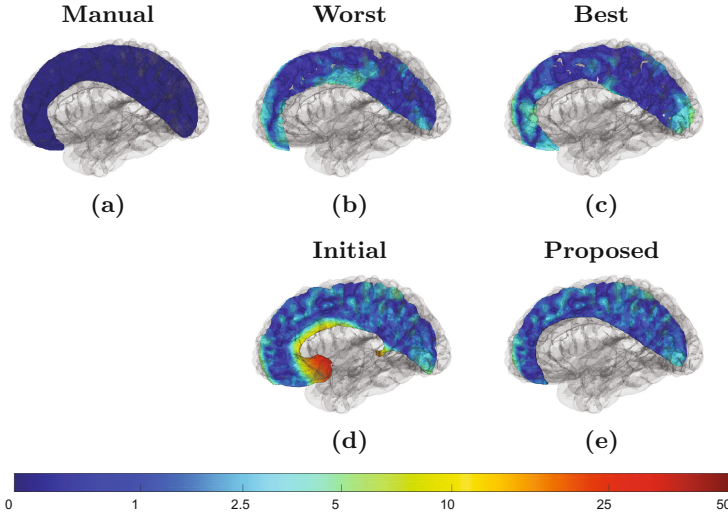
Fig. 4. 3D rendering of the falx showing **(a)** the manual delineation, the results of single atlas registration for the **(b)** worst and **(c)** best cases; **(d)** the initial falx estimate and **(e)** after refinement. The color of the surface indicates the distance in mm to the manual delineation on a log-scale.

sagittal plane and any voxel that lies outside the refined boundary is removed. A rendering showing the result before and after refinement is given in Fig. 4.

3   Results

The proposed method is applied to 23 subjects with five of the subjects selected as atlases for the multi-atlas boundary fusion. The manual delineation followed the protocol described in Sect. 2.1. To quantify the performance of the method, Hausdorff distance (HD) and mean surface distance (MSD) to the manual delineation is computed. HD finds the maximum of the minimum distances between two surfaces. To calculate the MSD, we compute the minimum distance at each voxel on one surface to the nearest voxel on the other surface and average across all voxels on both surfaces. HD and MSD are reported in mm. The method is compared with the initial falx estimate as computed in Sect. 2.1 and the result from using a single atlas. For the single atlas result, since there are five possible atlases to use for each subject, the best and worst results in terms of HD are reported in Table 1 and the number of times each atlas is used to produce those results is reported in Table 2. Finally, the median HD and MSD taken across the single atlas results is also reported.

From Table 1, we see that the refinement step in the proposed method improves the HD and MSD compared to our initial falx estimate, where the surface distance is largest in the inferior frontal falx. Furthermore, compared to a single atlas approach, the proposed method has a better HD and MSD than

Table 1. The mean Hausdorff distance (HD) and mean surface distance (MSD)—with standard deviations in parentheses—for the best, median, and worst cases of single subject registration, the initial falx estimate, and the proposed approach.

	HD (mm)	MSD (mm)
Single (Best)	8.33 (±1.88)	1.08 (±0.19)
Single (Median)	11.35 (±2.07)	1.16 (±0.17)
Single (Worst)	15.88 (±2.77)	1.38 (±0.31)
Initial falx	35.47 (±3.19)	2.28 (±0.39)
Proposed	9.67 (±2.61)	0.86 (±0.12)

Table 2. Number of times each atlas produced the best and worst single atlas result in terms of Hausdorff distance.

	Atlas 1	Atlas 2	Atlas 3	Atlas 4	Atlas 5
Best	1	0	9	6	7
Worst	8	11	0	2	2

the median and worst cases. The best case for the single atlas approach has a better HD, while the proposed approach has better MSD. The difference in HD and MSD for all methods compared to the proposed method is statistically significant using a paired Wilcoxen signed rank test with $p < 0.01$. However, the difficulty with single atlas approaches is that the atlas that produces the best case varies per subject, as shown in Table 2. Therefore, it is not realistic to expect the best case performance in all situations from the single atlas approach. The proposed approach leverages multiple atlases to minimize the effect of registration errors that might occur in any single atlas. 3D renderings of the results are provided in Fig. 4, which visually agree with conclusions from the HD and MSD results. We also note that when a single atlas is deformed, there is no guarantee that the result will be in the longitudinal fissure, while the proposed approach ensures that this is the case. The largest surface distances in the single atlas approaches occur in areas where the registration has moved the falx outside of the longitudinal fissure.

4   Conclusion

In this work, we propose an algorithm to segment the falx using T1-w MRI and SWI. We start with an initial falx and refine that estimate using a multi-atlas approach. The final falx contour is generated by fusing the contours from a set of atlases with manually delineated falxes that are put into the subject space by a deformable registration of the SWI. Point correspondence is generated using coherent point drift and the contours are fused using continuous-STAPLE. The proposed approach greatly improves Hausdorff distance compared to the initial

falx estimate and its performance falls between the best and worst cases for the single atlas approach. For the mean surface distance, our proposed approach is always better than the best single atlas case.

References

1. Adeeb, N., Mortazavi, M.M., Tubbs, R.S., Cohen-Gadol, A.A.: The cranial dura mater: a review of its history, embryology, and anatomy. Child's Nerv. Syst. **28**(6), 827–837 (2012)
2. Avants, B.B., Epstein, C.L., Grossman, M., Gee, J.C.: Symmetric diffeomorphic image registration with cross-correlation: evaluating automated labeling of elderly and neurodegenerative brain. Med. Image Anal. **12**(1), 26–41 (2008)
3. Chen, I., Coffey, A.M., Ding, S., Dumpuri, P., Dawant, B.M., Thompson, R.C., Miga, M.I.: Intraoperative brain shift compensation: accounting for dural septa. IEEE Trans. Biomed. Eng. **58**(3), 499–508 (2011)
4. Chen, I., Simpson, A.L., Sun, K., Thompson, R.C., Miga, M.I.: Sensitivity analysis and automation for intraoperative implementation of the atlas-based method for brain shift correction. In: Proceedings of SPIE, vol. 8671, pp. 86710T-1–86710T-12 (2013)
5. Chen, W., Smith, R., Ji, S.Y., Ward, K.R., Najarian, K.: Automated ventricular systems segmentation in brain CT images by combining low-level segmentation and high-level template matching. BMC Med. Inform. Decis. Making **9**(1), S4 (2009)
6. Claessans, M., Sauren, F., Wismans, J.: Modeling of the human head under impact conditions: a parametric study. In: Proceedings: Stapp Car Crash Conference, vol. 41, pp. 315–328 (1997)
7. Commowick, O., Warfield, S.K.: A continuous staple for scalar, vector, and tensor images: an application to DTI analysis. IEEE Trans. Med. Imaging **28**(6), 838–846 (2009)
8. Glaister, J., Carass, A., Pham, D.L., Butman, J.A., Prince, J.L.: Automatic falx cerebri and tentorium cerebelli segmentation from magnetic resonance images. In: Proceedings of SPIE Medical Imaging (SPIE-MI 2017), Orlando, FL, vol. 10137, pp. 101371D-1–101371D-7, 11–16 February 2017
9. Huo, Y., Plassard, A.J., Carass, A., Resnick, S.M., Pham, D.L., Prince, J.L., Landman, B.A.: Consistent cortical reconstruction and multi-atlas brain segmentation. NeuroImage **138**, 197–210 (2016)
10. Klein, A., Tourville, J.: 101 labeled brain images and a consistent human cortical labeling protocol. Front. Neurosci. **6**, 171 (2012)
11. Myronenko, A., Song, X.: Point set registration: coherent point drift. IEEE Trans. Pattern Anal. Mach. Intell. **32**(12), 2262–2275 (2010)
12. Ruan, J., Khalil, T., King, A.: Human head dynamic response to side impact by finite element modeling. J. Biomech. Eng. **113**(3), 276–283 (1991)
13. Voo, L., Kumaresan, S., Pintar, F.A., Yoganandan, N., Sances, A.: Finite-element models of the human head. Med. Biol. Eng. Comput. **34**(5), 375–381 (1996)
14. Wang, H., Suh, J.W., Das, S.R., Pluta, J.B., Craige, C., Yushkevich, P.A.: Multi-atlas segmentation with joint label fusion. IEEE Trans. Med. Imaging **35**(3), 611–623 (2013)